Nat Hazards (2015) 76:791–810
DOI 10.1007/s11069-014-1517-5

ORIGINAL PAPER

Seismic response of embankment slopes with different reinforcing measures in shaking table tests

Yu-liang Lin · Wu-ming Leng · Guo-lin Yang · Liang Li · Jun-Sheng Yang

Received: 5 June 2014 / Accepted: 4 November 2014 / Published online: 8 November 2014

Abstract In order to study the seismic response of the embankment slopes with different reinforcing measures, shaking table tests were performed on three embankment slope models (i.e., unreinforced embankment slope, 2-layer reinforced embankment slope and 4-layer reinforced embankment slope). Wenchuan earthquake motions and white noise excitations were performed to investigate the change of the model parameters, the horizontal acceleration response, the vertical acceleration response and the dynamic earth pressure response of embankment slopes. A comparison was made on the seismic response among the embankment slopes with different reinforcing measures. The results show that the natural frequency of reinforced embankment slope is larger than that of unreinforced embankment slope, and the reinforced embankment slope is less sensitive to seismic excitation. Horizontal acceleration response is obviously amplified by embankment slope. Horizontal acceleration magnification presents a decreasing trend with the increase of the peak value of input horizontal acceleration, and the decreasing ratio is higher for reinforced embankment slope. The vertical acceleration magnification of reinforced embankment slope is much smaller than that of unreinforced embankment slope, and the nonlinear characteristic of embankment slope in vertical direction is not as obvious as that in horizontal direction. Residual earth pressure is mainly induced at the upper part of embankment slope.

Keywords Seismic response · Embankment slope · Geogrid · Shaking table test

Y. Lin (✉) · W. Leng · G. Yang · L. Li · J.-S. Yang
School of Civil Engineering, Central South University, Changsha 410075, China
e-mail: linyuliang11@163.com

Y. Lin · W. Leng · G. Yang
National Engineering Laboratory for High Speed Railway Construction, Changsha 410075, China

1 Introduction

It is widely reported that a large number of earth embankments or slopes were damaged during the past great earthquakes (Omer and Resat 2002; Bakir and Akis 2005; Singh et al. 2005; Kamai and Sangawa 2011; Toyohiko et al. 2011; Huang et al. 2012a, 2013). In 2008, about 197,481 slope failures were triggered by Wenchuan earthquake of China (M_w 7.9 or M_s 8.0) (Xu and Xu 2013; Xu et al. 2014c), and the phenomena of seismic liquefaction and subsidence were also observed (Huang and Jiang 2010; Huang et al. 2011, 2012b, c). The Yushu, China, earthquake in 2010 (M_w 6.9) triggered more than 2,036 coseismic landslides with a total coverage area of 1.194 km^2 (Xu and Xu 2014). The Port-au-Prince, Haiti earthquake in 2010 (M_w7.0) induced more than 30,828 slope failures, which distributed in an area larger than 3,000 km^2, and covered about 15.736 km^2 with an estimated landslide erosion volume about 29,700,000 m^3 (Xu et al. 2014a). The Minxian–Zhangxian, China, earthquake in 2013 (M_w 5.9) triggered at least 2,330 slope failures (Xu et al. 2014b). The dynamic behavior of earth embankment or slope subjected to earthquake loading requires a further understanding for creating a safe seismic design.

Traditionally, the seismic stability of embankment or slope was analyzed by pseudostatic analysis method which simply added the seismic force to the static limit equilibrium analysis (Liu and Shi 2006; Shukha and Baker 2008; Munwar and Sivakumar 2009). The pseudostatic analysis method was widely used for seismic design in current codes for its briefness. The deformation control is another method for seismic design of embankment or slope. Newmark (1965) presented an analysis method by calculating the permanent displacement as a function of the critical acceleration, which was later well known as Newmark's sliding block method. Newmark's sliding block method is simple to apply in practice and it was greatly improved by many scholars (Chugh 1995; Crespellani et al. 2003; Hsieh and Lee 2011; Kim and Sitar 2013). However, the Newmark's sliding block method still presented some of crude assumptions of pseudostatic analysis (Jibson 2011).

The rapid development of centrifuge technique and shaking table apparatus makes it possible to study the seismic response of earth embankment or slope under real stress–strain condition in laboratory. In recent years, dynamic centrifuge tests or shaking table tests were widely adopted by scholars to investigate the seismic response of geotechnical structures (Mohajeri and Towhata 2003; Teymur and Madabhushi 2003; Kagawa et al. 2004; Rayhani and El Naggar 2007; Torisu et al. 2010; Motamed et al. 2013; Srilatha et al. 2013; Turan et al. 2013). In dynamic centrifuge test, the test model can well meet the requirements of similarity relation because the gravitational field can be changed as expected. However, the carrying capacity of dynamic centrifuge is very limited due to the complicated technology of centrifuge system, and most of the existing literatures mainly performed dynamic centrifuge test on small-scale model (Yu et al. 2008, 2010; Ha et al. 2014). Instead, the shaking table system can support a large-scale model with a wide loading frequency in despite of some shortages in similarity design. Liu et al. (2014) performed a series of large-scale shaking table model tests to evaluate the effectiveness of various reinforcing measures on concrete faced rock-fill dams. The dimension of the model is 4.0 m × 0.9 m × 1.5 m (length × width × height). Wang et al. (2010) conducted shaking table model tests to study the failure behavior of slope with a model dimension of 3.5 m × 1.5 m × 1.7 m under Wenchuan excitation with a conclusion that the tension cracks mainly emerged at the upper part of slope, while the bottom of slope nearly remained intact.

The seismic stability or engineering behavior of earth embankment or slope can be well improved by taking reinforcing measure, which is investigated both in field survey and laboratory test (Tatsuoka et al. 2007; Wang et al. 2011; Liu et al. 2012; Huang et al. 2006). For example, Sandri (1997) presented a summary of observations on retaining walls and reinforced soil slopes after Northridge earthquake, and the results showed that the reinforced structures performed excellently subjected to earthquake loading. Hong et al. (2005) performed shaking table tests on five-nailed model slopes, and the research showed that the nails could improve the seismic resistance of steep slopes notably. The previously published works promoted the application of reinforcing measure and developed the methods for seismic design of reinforced structure. However, an economic and effective reinforcing measure requires a comprehensive understanding on seismic response of different patterns of reinforced embankment or slope, which should be further studied.

In this work, large-scale shaking table model tests were carried out on three embankment slope models with different reinforcing measures (i.e., unreinforced embankment slope, 2-layer reinforced embankment slope and 4-layer reinforced embankment slope). Wenchuan earthquake motions and white noise excitations were mainly performed in the test to investigate the seismic response of embankment slopes including the change of model parameter, the horizontal acceleration response, the vertical acceleration response and the dynamic earth pressure response. The seismic response among the embankment slopes with different reinforcing measures was also compared.

2 Shaking table tests

2.1 Similarity laws and materials

Shaking table tests were performed on large-scale shaking table established at China Merchants Chongqing Communications Research and Design Institute Co. Ltd, which was equipped with electro-hydraulic servo-controlled system. The dimension of the table is 6 m × 3 m (length × width). The shaking table system can support the test model with the weight of 350 kN and provide a loading frequency of 0.1–50 Hz.

Shaking table test model was designed based on the prototype of single-line unballasted track railway embankment slope, which was constructed on rock foundation. According to the dimension of prototype and the capacity of shaking table system, the similarity ratio of geometry size was determined to be 1:8. Taking the parameters including geometry size, mass density and gravity acceleration as control variables, the similarity laws for embankment slope can be deduced based on Buckingham π theory with the assumption that the soil obeys Mohr–Coulomb criterion in static condition and equivalent viscoelastic criterion in dynamic condition (Iai 1989; Lin and Wang 2006; Wang et al. 2010; Lin 2013a, b; Lin and Yang 2013). The similarity laws of embankment slope are shown in Table 1. In which, input acceleration and time were set as input control variables in shaking table test.

The soil used in shaking table tests was obtained from a deposit in Chongqing city, China. Based on grading analysis test, the non-uniform coefficient and curvature coefficient of the soil were 11.5 and 1.04, respectively. The soil was defined as "A-filler" according to the "Code for Design on Subgrade of Railway" (GB10001-2005) in China. The cohesion and internal friction angle of the soil were 11.2 kPa and 24.3°. The optimum water content and the maximum dry unit weight were 8.44 % and 20.2 kN/m^3. Bi-directional geogrid of TGSG25-25 was used in reinforced embankment slopes. According to tensile test, the longitudinal and

Table 1 Similarity laws of embankment slope in shaking table test

Physical variables	Similarity law	Similarity constants	Remarks
Geometry (l)	C_l	8	Control variable
Mass density (ρ)	C_ρ	1	Control variable
Gravity acceleration (g)	C_g	1	Control variable
Input acceleration (a)	C_a	1	Input control
Stress (σ)	$C_\sigma = C_\rho C_l$	8	
Cohesion (c)	$C_c = C_\rho C_l$	8	
Internal friction angle (φ)	C_φ	1	
Interface friction angle (δ)	C_δ	1	
Time (t)	$C_t = C_\rho^{1/4} C_l^{3/4}$	4.76	Input control
Frequency (f)	$C_f = C_\rho^{-1/4} C_l^{-3/4}$	0.21	
Damping ratio (ζ)	C_ζ	1	

transverse tensile strengths of the geogrid were 26.0 and 25.1 kN/m. The longitudinal and transverse elongations were 15.0 and 12.0 %, respectively.

2.2 Test cases and input excitations

Three groups of shaking table test were performed on embankment slopes with different reinforcing measures, and they were code-named unreinforced embankment slope, 2-layer reinforced embankment slope and 4-layer reinforced embankment slope, respectively. Every embankment slope model was constructed in a special model box with a dimension of 3.6 m × 1.5 m × 2.0 m (length × width × height). According to the similarity laws of embankment slope, rock foundation was simulated by concrete layer with a thickness of 0.4 m at the bottom of model box. The embankment body and bottom layer were designed to be 1.2 and 0.3 m in height, respectively. The graded gravel board was determined to be 0.1 m in height with a consideration of the counterweight of upper structure on railway embankment, as shown in Fig. 1. The compaction degrees of embankment body and bottom layer were 87 and 95 %, respectively. In 2-layer reinforced embankment slope, two pieces of TGSG25-25 geogrid were laid in the elevations of 0.5 and 1.0 m to rock foundation. In 4-layer reinforced embankment slope, four pieces of TGSG25-25 geogrid were laid in the elevations of 0.3, 0.6, 0.9 and 1.0 m to rock foundation. The length of geogrid was all designed to be 1.0 m, as shown in Table 2. A photograph of embankment slope model on shaking table is shown in Fig. 2.

In order to reduce the "box-effect" in shaking table test, the natural frequency of the model box should not be close to that of the soil. In this paper, the model box was diagonally supported by U-steel on two sides to improve the stiffness of the model box, which subsequently increased the natural frequency of the model box. The results showed that the natural frequency of the model box reached 120 Hz, which was much larger than that of the soil. Polystyrene foam board was set inside the model box to reduce the wave reflection during the test. More details about the model box, the soil and the embankment model were described by Lin and Yang (2013).

The characteristic of near-field ground motion is greatly different from that of far-field motion, and the structure will be more vulnerable subjected to near-field ground motion (Alavi and Krawinkler 2004; Chopra and Chintanapakdee 2001a, b; Yaghmaei-Sabegha

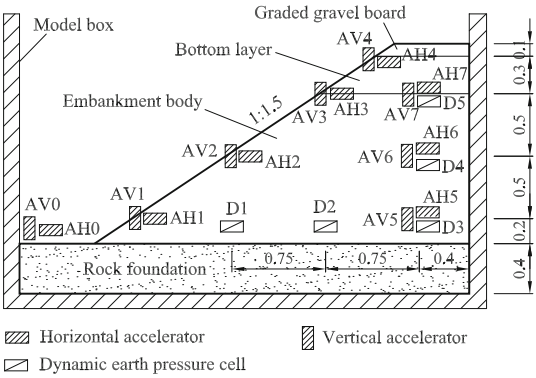

Fig. 1 Embankment slope model and instruments layout (unit: m)

and Tsang 2011; Davoodi et al. 2013). Consequently, Wenchuan earthquake motion, which was the nearest ground motion data recorded at Wolong station in Wenchuan earthquake in 2008, was selected for test. Wenchuan earthquake motion was a long-period pulse with two great impulsions. The timeline of Wenchuan earthquake motion was compressed according to the time similarity constant ($C_t = 4.76$) in shaking table test. The time history and the Fourier spectrum of compressed Wenchuan earthquake motion are shown in Fig. 3. The Wenchuan earthquake motion was performed in bi-direction during the test. The horizontal peak acceleration of Wenchuan excitation was adjusted to 0.1, 0.2, 0.4, 0.6, 0.8 and 1.0 g, respectively. Correspondingly, the vertical peak acceleration was adjusted to 2/3 of horizontal peak acceleration for each Wechuan excitation. White noises with peak acceleration of 0.03–0.05 g were performed among Wenchuan excitations to investigate the change of the modal parameters of embankment slopes. The loading method of shaking table test is shown in Table 3. In which, Wenchuan excitation was code-named WCXZ, and white noise was code-named WN. Three groups of shaking table tests shared a same loading method.

2.3 Instruments and measurements

The sensors including accelerometers and dynamic earth pressure cells were used in shaking table test. The type of accelerometer was CA-YD-189. The measuring range and the frequency range of accelerometer were ±0.5 g and 0.2–1,000 Hz, respectively. Accelerometers were laid in slope surface and mid-section of embankment slope in both horizontal and vertical directions. The mid-section was a vertical plane which was about 0.4 m distance from the backside of model box. The horizontal accelerometers in slope surface and mid-section were upwards numbered as AH1–H4 and AH5–AH7, respectively. The vertical accelerometers in slope surface and mid-section were upwards numbered as AV1–V4 and AV5–AV7, respectively. Additional, one horizontal accelerometer and another vertical accelerometer were set on rock foundation, and they were numbered as AH0 and AV0, respectively, as shown in Fig. 1.

The type of dynamic earth pressure cell used in the test was BX-7 with a measuring range of 0.1–100 kPa. Three dynamic earth pressure cells were laid in mid-section, and they were upwards numbered as D3, D4 and D5. Another two dynamic earth pressure cells were laid in a horizontal plane which was 0.2 m elevation to rock foundation, and they were numbered as D1 and D2, as shown in Fig. 1.

Table 2 Summary of different patterns of reinforced embankment slopes

Cases	Reinforced layers	Slope angle	Slope height (m)	Distance of the nearest geogrid to foundation (m)	Geogrid spacing (m)	Geogrid length (m)	Compaction degree of embankment body (%)	Compaction degree of bottom layer (%)
Unreinforced	0	33.7°	1.5	–	–	–	87	95
2-layer	2	33.7°	1.5	0.5	0.5	1	87	95
4-layer	4	33.7°	1.5	0.3	0.3	1	87	95

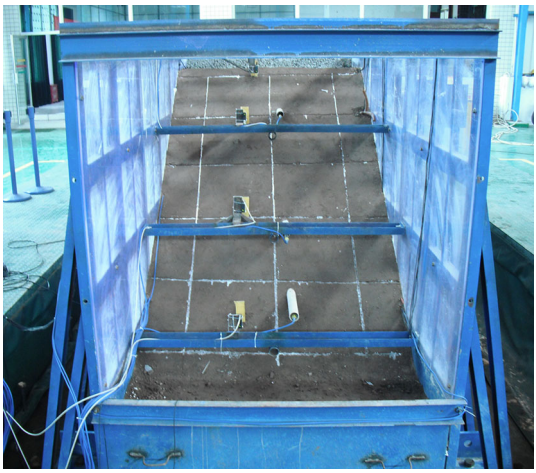

Fig. 2 An embankment slope model on shaking table

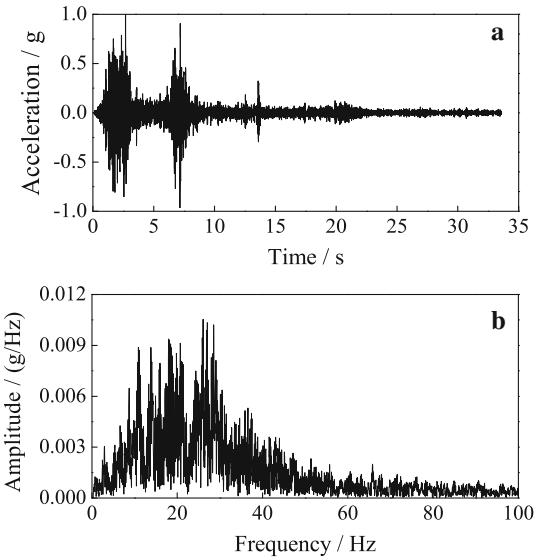

Fig. 3 Time history **(a)** and Fourier spectrum **(b)** of compressed Wenchuan earthquake motion in shaking table test

Both acceleration response and dynamic earth pressure response were collected by Dewetron 2010 Data Acquisition System, and the sampling frequency was 2,000 Hz.

3 Modal parameters of embankment slope

The modal parameters of embankment slope mainly include natural frequency and damping ratio. The change of modal parameters can sensitively reflect the effect of seismic excitation on embankment slope. In this work, the modal parameters of embankment slope were determined by Transfer Function Method based on the acceleration response in slope surface under white noise excitations. Transfer Function Method is a widely used method

Table 3 Loading method in shaking table test

Serial number	Code name of operation conditions	Peak acceleration/g	
		x	z
1	WN1	0.03	0.03
2	WCXZ1	0.1	0.07
3	WN2	0.03	0.03
4	WCXZ2	0.2	0.13
5	WN3	0.03	0.03
6	WCXZ3	0.4	0.27
7	WN4	0.05	0.05
8	WCXZ4	0.6	0.40
9	WN5	0.05	0.05
10	WCXZ5	0.8	0.53
11	WN6	0.05	0.05
12	WCXZ6	1.0	0.67
13	WN7	0.05	0.05

in Frequency Domain Identification Analysis. The transfer function $H_a(i\omega)$ can be determined as following for shaking table test:

$$H_a(i\omega) = \frac{S_{xy}(i\omega)}{S_x(\omega)} \tag{1}$$

In which, $S_{xy}(i\omega)$ is the cross spectral density function between the acceleration response of test point and the acceleration response on rock foundation; $S_x(\omega)$ is the self-power spectral density function of acceleration response. The natural frequency and damping ratio can be determined by amplitude analysis method based on the results of transfer function $H_a(i\omega)$.

Figures 4 and 5 show the change of modal parameters in both horizontal and vertical directions during the test. The natural frequency of reinforced embankment slope is larger than that of unreinforced embankment slope, and the natural frequency of 4-layer reinforced embankment slope is also larger than that of 2-layer reinforced embankment slope. Geogrids in embankment slope can increase the natural frequency of embankment slope and reduce its damping ratio. The interface friction function between geogrid and soil can restrict the deformation of soil and improve the shear modulus of embankment slope. Thus, the seismic stability of reinforced embankment slope can be improved.

No matter whether the embankment slope is reinforced or not, the natural frequency of embankment slope in both horizontal and vertical directions presents a decreasing trend during the test. Contrarily, the damping ratio exhibits an increasing trend although the test results of damping ratio are somewhat scattered. Such phenomenon reflects that the shear modulus of the embankment slope decreases, and the soil is somewhat loosened during the test. With the increase of excitations, the decreasing ratio of the natural frequency of unreinforced embankment slope is larger than that of reinforced embankment slope. For example, the initial natural frequency of unreinforced embankment slope is 24.0 Hz under WN1 condition. After the test, the natural frequency of unreinforced embankment slope is 18.8 Hz under WN9 condition with a decreasing ratio of 21.7 %. The natural frequency of 4-layer reinforced embankment slope decreases from 25.7 to 22.2 Hz with the decreasing ratio of 13.6 % during the test. It is seen that the reinforced embankment slope is less sensitive to seismic excitation than the unreinforced embankment slope.

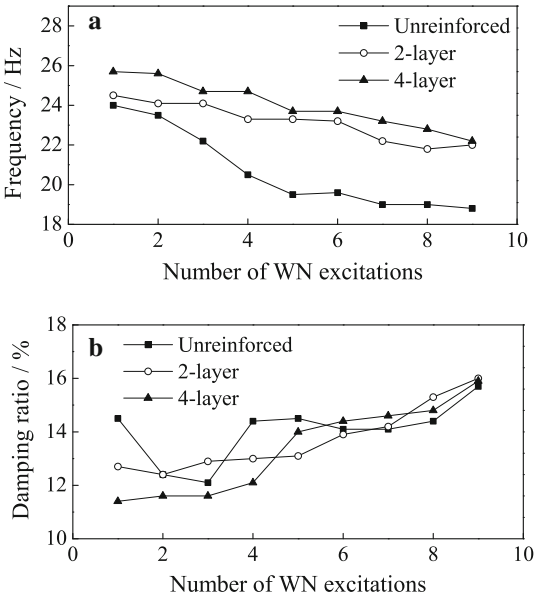

Fig. 4 First-order natural frequency **(a)** and damping ratio **(b)** of embankment slopes in horizontal direction

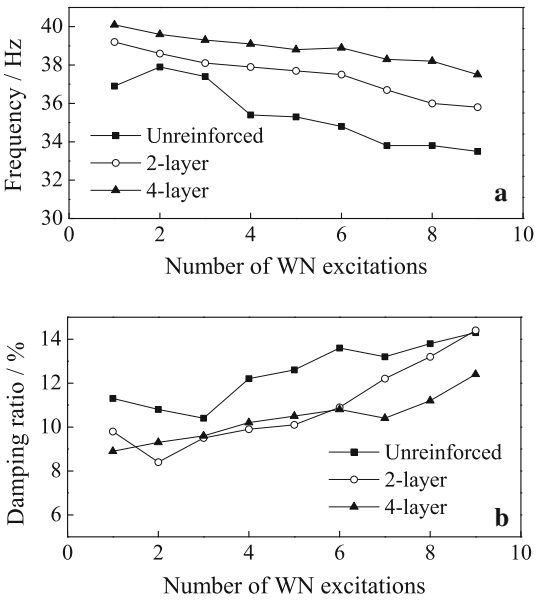

Fig. 5 First-order natural frequency **(a)** and damping ratio **(b)** of embankment slopes in vertical direction

4 Horizontal acceleration response

Acceleration magnification is widely used to evaluate the acceleration response of embankment slope. The pseudo-static method for seismic design in current codes is developed based on the information of acceleration magnification. In this work, acceleration magnification is defined as the ratio of the peak value of the acceleration response in embankment slope to the peak value of the acceleration on rock foundation. The

distributions of horizontal acceleration magnification are shown in Fig. 6. The horizontal acceleration magnification is always larger than 1.0, and the embankment slope presents obvious amplification effect on input excitations. The horizontal acceleration magnification increases along the height of embankment slope, and the increasing ratio increases at the top of embankment slope, especially when the horizontal acceleration of input excitation is larger than 0.8 g. It is inferred that reinforcing effect at the top of embankment slope should be enhanced to restrict the deformation of soil, especially in the areas of high seismic intensity. However, the difference of horizontal acceleration magnification distribution is not obvious among the different patterns of reinforced embankment slopes.

Figure 7 shows the relationship between the horizontal acceleration magnification and the input horizontal peak acceleration for different test points. Horizontal acceleration magnification differs under the Wenchuan excitations of different intensities. Generally, the horizontal acceleration magnification presents a decreasing trend with the increase of horizontal peak acceleration. According to the research of Lin and Yang (2013), logarithmic function is recommended to describe such relationship:

$$\mathrm{RATIO} = a + b\ln(A_{x\max}) \tag{2}$$

In which, RATIO represents the horizontal acceleration magnification; $A_{x\max}$ represents the peak value of input horizontal acceleration; a and b are fitting parameters. The fitting results for several test points are shown in Table 4. It is seen that the fitting parameter b is always negative, which reflects the decreasing trend of RATIO with the increase of $A_{x\max}$. The absolute value of b reflects the decreasing speed of RATIO. It is seen that RATIO of reinforced embankment slope (both 2-layer and 4-layer reinforced embankment slope) decreases more quickly than that of unreinforced embankment slope with the increase of $A_{x\max}$, which means that the reinforced embankment slope will present a weaker ground motion than unreinforced embankment slope under an equal strong seismic excitation. The result is also validated in Fig. 8, which shows the typical acceleration time history of point AH4 for both 4-layer reinforced embankment slope and unreinforced embankment slope under WCXZ6 condition ($A_{x\max} = 1.0$ g). The maximum horizontal acceleration response of 4-layer reinforced embankment slope is about 1.468 g, which is about 51.7 % of that of unreinforced embankment slope. The interface friction function between geogrid and soil can reduce the acceleration response of embankment slope, especially when the seismic excitation is strong. Consequently, it is an effective way to improve the seismic stability of embankment slope by taking reinforcing measure.

5 Vertical acceleration response

Most of previously published works mainly focus on the research of horizontal acceleration response for the consideration that the horizontal seismic function will induce greater damage to structure than the vertical seismic excitation. However, the vertical inertia force exists with large intensity for many cases, and it is also a main factor that results in the damage of structure especially in meizoseismal areas.

Figure 9 shows the distribution of the vertical acceleration magnification under Wenchuan excitations of different intensities. In which, $A_{z\max}$ refers to the peak value of input vertical acceleration. Like horizontal acceleration magnification, the vertical acceleration magnification increases along the height of embankment slope. However, the value of vertical acceleration magnification is much smaller than that of horizontal acceleration

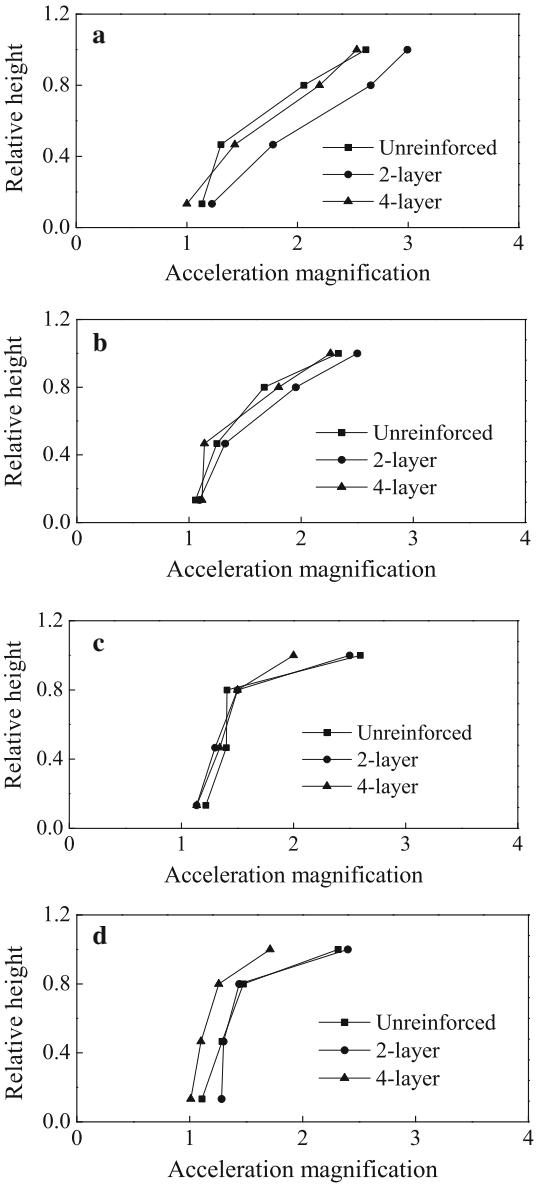

Fig. 6 Distributions of horizontal acceleration magnification under Wenchuan excitations of different intensities. **a** WCXZ2 ($A_{x\max} = 0.2$ g). **b** WCXZ3 ($A_{x\max} = 0.4$ g). **c** WCXZ5 ($A_{x\max} = 0.8$ g). **d** WCXZ6 ($A_{x\max} = 1.0$ g)

magnification, and the vertical acceleration magnification is even less than 1.0 at the bottom of embankment slope for some excitation conditions. For example, the range of vertical acceleration magnification of 2-layer reinforced embankment slope is 0.86–1.80 under WCXZ3 condition, while the range of horizontal acceleration magnification is 1.06–2.33. Such phenomenon can be well explained in frequency domain. By making Fourier transform on compressed Wenchuan earthquake motion, it is seen that the significant frequency band of compressed Wenchuan earthquake motion is mainly concentrated at 10–30 Hz, as shown in Fig. 3. According to the test results of modal parameters,

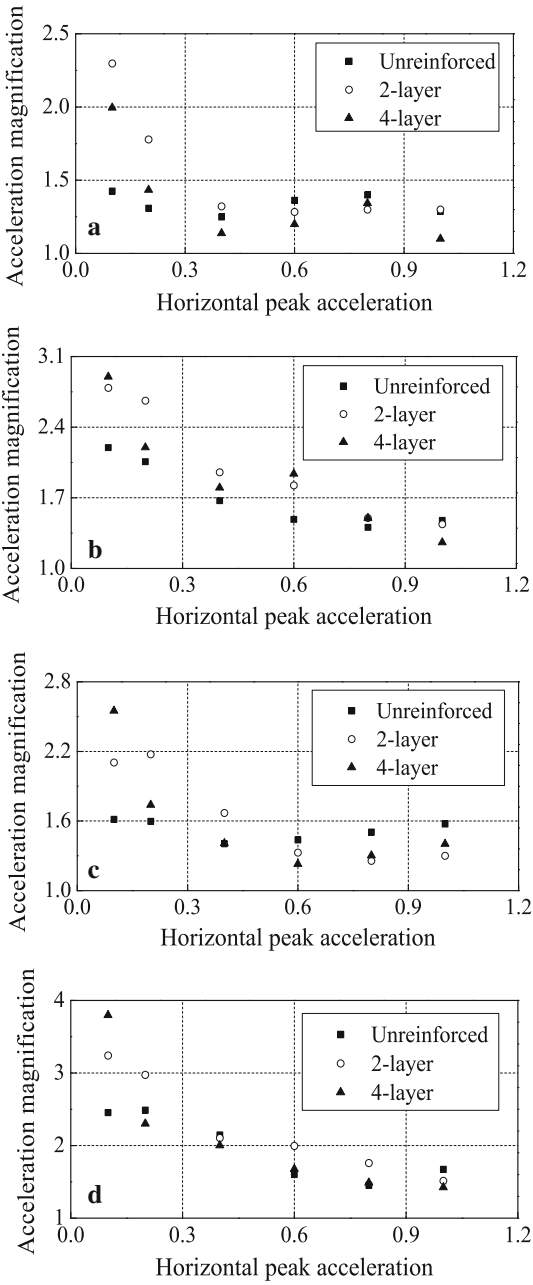

Fig. 7 Relationship between horizontal acceleration magnification and input horizontal peak acceleration for typical test points. **a** Point AH2. **b** Point AH3. **c** Point AH6. **d** Point AH7

the range of the horizontal natural frequency of 2-layer reinforced embankment slope is 22.0–24.5 Hz, and the range of the vertical natural frequency is 35.8–39.2 Hz, as shown in Figs. 4 and 5. The significant frequency of compressed Wenchuan earthquake motion well covers the horizontal natural frequency of the embankment slope, which will induce a

Table 4 Fitting results for the relationship between horizontal acceleration magnification and the peak value of input horizontal acceleration

Cases	Fitting parameters	Test points in slope surface			Test points in mid-section	
		AH2	AH3	AH4	AH6	AH7
Unreinforced	*a*	1.316	1.374	2.367	1.480	1.538
	b	−0.025	−0.369	−0.173	−0.046	−0.466
2-layer	*a*	1.140	1.435	2.424	1.229	1.551
	b	−0.439	−0.639	−0.386	−0.442	−0.770
4-layer	*a*	1.071	1.350	1.706	1.140	1.231
	b	−0.321	−0.629	−0.806	−0.502	−0.954

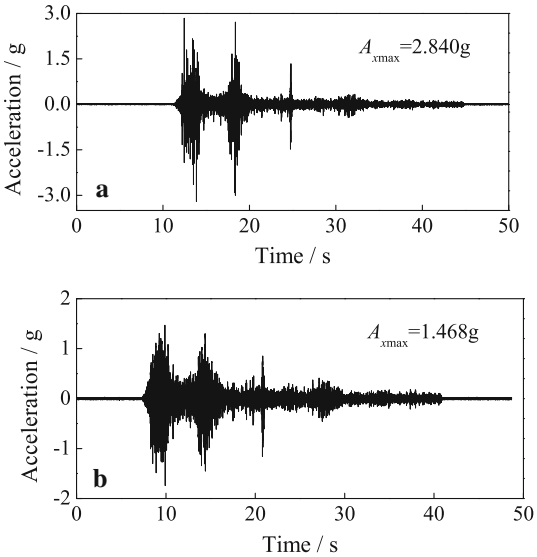

Fig. 8 Horizontal acceleration time history of point AH4 for unreinforced embankment slope **(a)** and 4-layer reinforced embankment slope **(b)** under WCXZ6 condition

resonance phenomenon, and subsequently induces a great acceleration magnification effect in horizontal direction.

Figure 10 shows the typical vertical acceleration time histories (i.e., point AH4) for both unreinforced embankment slope and 4-layer reinforced embankment slope under WCXZ6 condition. The peak value of the vertical acceleration response of 4-layer reinforced embankment slope is 1.179 g, which is about 48.1 % of that of unreinforced embankment slope. The geogrid can reduce the magnification effect of vertical acceleration response. When the seismic wave transmits upwards along the embankment slope, the geogrid exists in embankment slope like a barrier, and the interface friction function between geogrid and soil can partly dissipate the seismic energy. Besides, it is also seen that the geogrid performs more obvious reduction effect on vertical acceleration response than that on horizontal acceleration response.

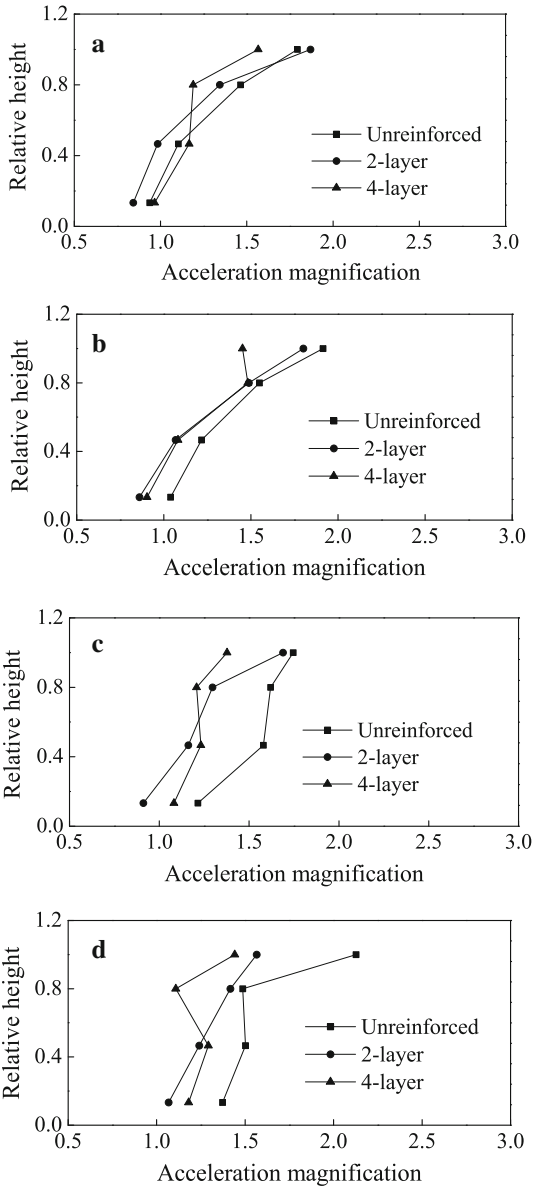

Fig. 9 Distributions of vertical acceleration magnification under Wenchuan excitations of different intensities. **a** WCXZ2 ($A_{zmax} = 0.13$ g). **b** WCXZ3 ($A_{zmax} = 0.27$ g). **c** WCXZ5 ($A_{zmax} = 0.53$ g). **d** WCXZ6 ($A_{zmax} = 0.67$ g)

Figure 11 shows the relationship between the vertical acceleration magnification and the peak value of input vertical acceleration for several test points. Unlike horizontal acceleration magnification, vertical acceleration magnification presents an increasing trend with the increase of excitation intensity for most test points. A linear-elastic system with linear damping will present a constant acceleration magnification regardless of the intensity of excitation. It is seen that the soil presents nonlinear characteristic in vertical direction. However, the acceleration magnification in vertical direction does not change as

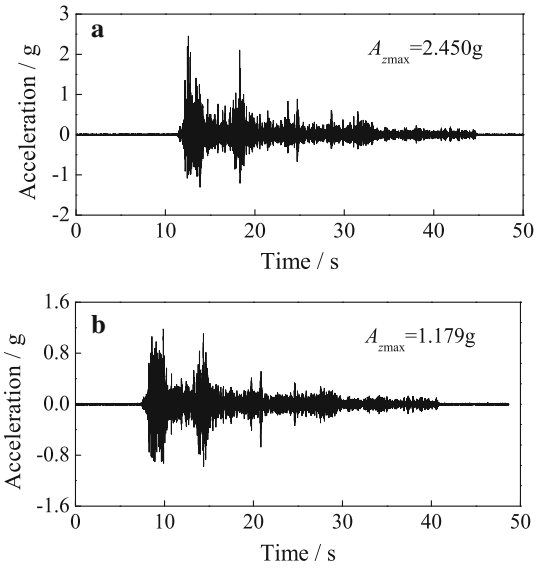

Fig. 10 Vertical acceleration time history of point AH4 for unreinforced embankment slope **(a)** and 4-layer reinforced embankment slope **(b)** under WCXZ6 condition

greatly as that in horizontal direction with the increase of input acceleration. The nonlinear characteristic in vertical direction is not as obvious as that in horizontal direction.

6 Dynamic earth pressure response

The representative study is made on the dynamic earth pressure response of several test points in 4-layer reinforced embankment slope under WCXZ4 condition, as shown in Fig. 12. The initial earth pressure caused by self-weight of soil is removed to analyze only the dynamic component of earth pressure. The baseline of dynamic earth pressure history fluctuates twice under Wenchuan excitation, which induces the residual earth pressure in embankment slope. The fluctuation of point D5 is most obvious and the vertical earth pressure in this zone is enhanced. The residual earth pressure will probably induce a new deformation in embankment slope. Consequently, the stiffness of the upper part of embankment slope should be enhanced, and the compaction degree of the soil should be highly required. Additionally, it is seen that the first fluctuation of the baseline of dynamic earth pressure response is greater than the second fluctuation. It is inferred that the residual earth pressure will be induced by strong ground excitation, and the value of residual earth pressure will be smaller when the embankment slope experiences another equal excitation.

Figure 13 compares the dynamic earth pressure response of point D5 in both unreinforced embankment slope and 2-layer reinforced embankment slope. Like point D5 in 4-layer reinforced embankment slope (as shown in Fig. 12d), the baseline of dynamic earth pressure response fluctuates obviously, and the vertical static earth pressure is enhanced. Meanwhile, it is seen that the intensity of dynamic earth pressure response of reinforced embankment slope is much weaker than that of unreinforced embankment slope. The peak values of dynamic earth pressure response of unreinforced embankment slope, 2-layer reinforced embankment slope and 4-layer reinforced embankment slope are 8.09, 5.05 and 4.99 kPa, respectively, and the ratio is about 1.6:1.0:1.0.

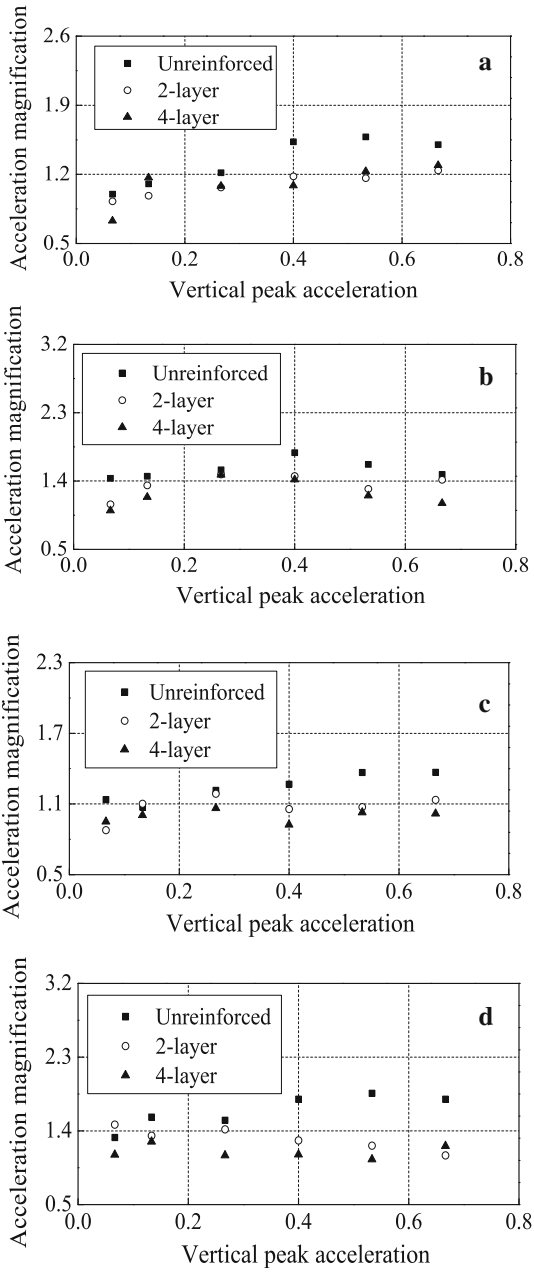

Fig. 11 Relationship between vertical acceleration magnification and the peak value of input vertical acceleration for typical test points. **a** Point AV2. **b** Point AV3. **c** Point AV6. **d** Point AV7

7 Conclusions

The natural frequency of embankment slope presents a decreasing trend during the test, and the damping ratio exhibits an increasing trend. The natural frequency of reinforced

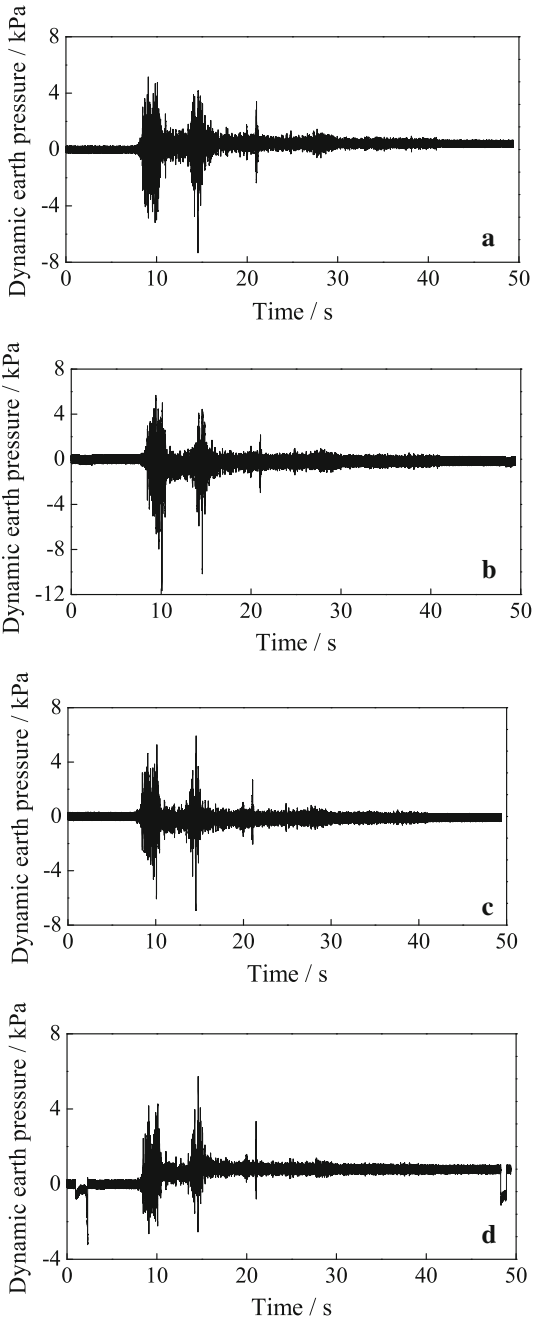

Fig. 12 Dynamic earth pressure response of the typical test points in 4-layer reinforced embankment slope under WCXZ4 condition. **a** Point D1. **b** Point D3. **c** Point D4. **d** Point D5

embankment slope is larger than that of unreinforced embankment slope under the same seismic condition. The reinforced embankment slope is less sensitive to seismic excitation than unreinforced embankment slope.

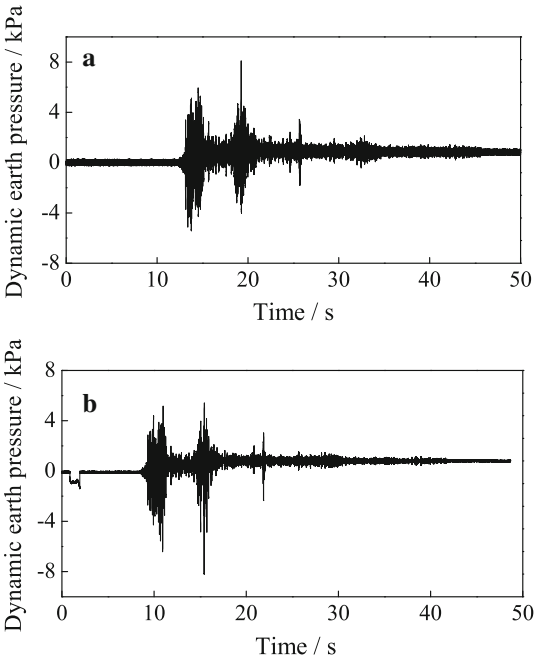

Fig. 13 Dynamic earth pressure response of Point D5. **a** Unreinforced embankment slope. **b** 2-Layer reinforced embankment slope

Horizontal acceleration response is obviously amplified by embankment slope. The horizontal acceleration magnification increases along the height of embankment slope with a higher increasing ratio at the top of embankment slope. Horizontal acceleration magnification presents a decreasing trend with the increase of excitation intensity, and the decreasing ratio of reinforced embankment slope is higher than that of unreinforced embankment slope.

Vertical acceleration magnification is much smaller than horizontal acceleration magnification because the significant frequency band of compressed Wenchuan earthquake motion does not well cover the vertical nature frequency of embankment slope. The vertical acceleration magnification of reinforced embankment slope is much smaller than that of unreinforced embankment slope, especially under the strong ground motion. The nonlinear characteristic of embankment slope in vertical direction is not as obvious as that in horizontal direction.

Residual earth pressure induced by seismic excitation mainly occurs at the upper part of the embankment slope. The intensity of dynamic earth pressure response of the reinforced embankment slope is weaker than that of the unreinforced embankment slope.

Acknowledgments This work is financially supported by the National Natural Science Foundation of China (51308551), the China Postdoctoral Science Foundation Funded Project (2012M511760), the Hunan Provincial Natural Science Foundation of China (13JJ4017) and the Fundamental Research Funds for the Central Universities of China (2012QNZT051).

References

Alavi B, Krawinkler H (2004) Behaviour of moment resisting frame structures subjected to near-fault ground motions. Earthq Eng Struct Dyn 33(6):687–706

Bakir BS, Akis E (2005) Analysis of a highway embankment failure associated with the 1999 Duzce Turkey earthquake. Soil Dyn Earthq Eng 25(3):251–260
Chopra AK, Chintanapakdee C (2001a) Comparing response of SDF systems to near-fault and far-fault earthquake motions in the context of spectral regions. Earthq Eng Struct Dyn 30(12):1769–1789
Chopra AK, Chintanapakdee C (2001b) Drift spectrum versus modal analysis of structural response to near-fault ground motions. Earthq Spectra 17(2):221–234
Chugh AK (1995) Dynamic displacement analysis of embankment dams. Geotechnique 45(2):295–299
Crespellani T, Facciorusso J, Madiai C, Vannucchi G (2003) Influence of uncorrected accelerogram processing techniques on Newmark's rigid block displacement evaluation. Soil Dyn Earthq Eng 23(6):415–424
Davoodi M, Jafari MK, Hadiani N (2013) Seismic response of embankment dams under near-fault and far-field ground motion excitation. Eng Geol 158:66–76
Ha JG, Lee SH, Kim DS, Choo YW (2014) Simulation of soil-foundation-structure interaction of Hualien large-scale seismic test using dynamic centrifuge test. Soil Dyn Earthq Eng 61(62):176–187
Hong YS, Chen RH, Wu CS, Chen JR (2005) Shaking table tests and stability analysis of steep nailed slopes. Can Geotech J 42(5):1264–1279
Hsieh SY, Lee CT (2011) Empirical estimation of the Newmark displacement from the Arias intensity and critical acceleration. Eng Geol 122(1–2):34–42
Huang Y, Jiang XM (2010) Field-observed phenomena of seismic liquefaction and subsidence during the 2008 Wenchuan earthquake in China. Nat Hazards 54(3):839–850
Huang Y, Sawada K, Moriguchi S, Yashima A, Zhang F (2006) Numerical assessment of the effect of reinforcement on the performance of reinforced soil dikes. Geotext Geomembr 24(3):169–174
Huang Y, Zhang WJ, Mao WW, Jin C (2011) Flow analysis of liquefied soils based on smoothed particle hydrodynamics. Nat Hazards 59(3):1547–1560
Huang Y, Zhang WJ, Xu Q, Xie P, Hao L (2012a) Run-out analysis of flow-like landslides triggered by the Ms 8.0 2008 Wenchuan earthquake using smoothed particle hydrodynamics. Landslides 9(2):275–283
Huang Y, Zheng H, Zhuang ZJ (2012b) Seismic liquefaction analysis of a reservoir dam foundation in the South-North Water Diversion project in China. Part I: liquefaction potential assessment. Nat Hazards 60(3):1299–1311
Huang Y, Zheng H, Zhuang ZJ (2012c) Seismic liquefaction analysis of a reservoir dam foundation in the South-North Water Diversion project in China. Part II: seismic response simulation. Nat Hazards 60(3):1313–1324
Huang RQ, Zhao JJ, Ju NP (2013) Analysis of an anti-dip landslide triggered by the 2008 Wenchuan earthquake in China. Nat Hazards 68(2):1021–1039
Iai S (1989) Similitude for shaking table tests on soil-structure fluid model in 1-g gravitational field. Soils Found 29(1):105–118
Jibson RW (2011) Methods for assessing the stability of slopes during earthquakes-A retrospective. Eng Geol 122(1–2):43–50
Kagawa T, Sato M, Minowa C, Abe A, Tazoh T (2004) Centrifuge simulations of large-scale shaking table tests: case studies. J Geotech Geoenviron Eng 130(7):663–672
Kamai T, Sangawa A (2011) Landslides on ancient embankments in the Kinki district (Japan): strong motion seismoscope of the 1596 Keichou-Fushimi earthquake. Quaternary Int 242(1):90–105
Kim JM, Sitar N (2013) Probabilistic evaluation of seismically induced permanent deformation of slopes. Soil Dyn Earthq Eng 44:67–77
Lin YL (2013a) Deformation behavior of reinforced embankment slopes under seismic excitation. Disaster Adv 6(7):12–19
Lin YL (2013b) Shaking table modeling of embankment slope response to earthquake loading. Disaster Adv 6(12):69–77
Lin ML, Wang KL (2006) Seismic slope behavior in a large-scale shaking table model test. Eng Geol 86(2):118–133
Lin YL, Yang GL (2013) Dynamic behavior of railway embankment slope subjected to seismic excitation. Nat Hazards 69(1):219–235
Liu RS, Shi HB (2006) An improved pseudo-static method for seismic resistant design of underground structures. Earthq Eng Eng Vib 5(2):189–193
Liu CN, Yang KH, Ho YH, Chang CM (2012) Lessons learned from three failures on a high steep geogrid-reinforced slope. Geotext Geomembr 34:131–143
Liu J, Liu FH, Kong XJ, Yu L (2014) Large-scale shaking table model tests of aseismic measures for concrete faced rock-fill dams. Soil Dyn Earthq Eng 61(62):152–163
Mohajeri M, Towhata I (2003) Shake table tests on residual deformation of sandy slopes due to cyclic loading. Soils Found 43(6):91–106

Motamed R, Towhata I, Honda T, Tabata K, Abe A (2013) Pile group response to liquefaction-induced lateral spreading: E-Defense large shake table test. Soil Dyn Earthq Eng 51:35–46
Munwar B, Sivakumar B (2009) Earthquake resistant design of reinforced soil structures using pseudo static method. Am J Eng Appl Sci 2(3):565–572
Newmark NM (1965) Effects of earthquakes on dams and embankments. Geotechnique 15:139–159
Omer A, Resat U (2002) Back-analysis of a seismically induced highway embankment failure during the 1999 Duzce earthquake. Environ Geol 42(6):621–631
Rayhani MHT, El Naggar MH (2007) Centrifuge modeling of seismic response of layered soft clay. Bull Earthq Eng 5(4):571–589
Sandri D (1997) A performance summary of reinforced soil structures in the greater Los Angeles area after the Northridge earthquake. Geotext Geomembr 15(4–6):235–253
Shukha R, Baker R (2008) Design implications of the vertical pseudo-static coefficient in slope analysis. Comput Geotech 35(1):86–96
Singh R, Roy D, Jain SK (2005) Analysis of earth dams affected by the 2001 Bhuj Earthquake. Eng Geol 80(3–4):282–291
Srilatha N, Latha MG, Puttappa CG (2013) Effect of frequency on seismic response of reinforced soil slopes in shaking table tests. Geotext Geomembr 36:27–32
Tatsuoka F, Tateyama M, Matsushima K (2007) Remedial treatment of soil structures using geosynthetic-reinforcing technology. Geotext Geomembr 25(4–5):204–220
Teymur B, Madabhushi SPG (2003) Experimental study of boundary effects in dynamic centrifuge modeling. Geotechnique 53(7):655–663
Torisu SS, Sato J, Towhata I, Honda T (2010) 1-G model tests and hollow cylindrical torsional shear experiments on seismic residual displacements of fill dams from the viewpoint of seismic performance-based design. Soil Dyn Earthq Eng 30(6):423–437
Toyohiko M, Daisuke H, Hiroshi Y, Shoji D, Noriyuki C, Jun U, Go S (2011) Reconnaissance report on landslide disasters in northeast Japan following the M 9 Tohoku earthquake. Landslides 8(3):339–342
Turan A, Hinchberger SD, El Naggar MH (2013) Seismic soil-structure interaction in buildings on stiff clay with embedded basement stories. Can Geotech J 50(8):858–873
Wang JA, Yao LK, Hussain A (2010) Analysis of earthquake-triggered failure mechanisms of slopes and sliding surfaces. J Mt Sci-Engl 7(3):282–290
Wang LP, Zhang G, Zhang JM (2011) Centrifuge model tests of geotextile-reinforced soil embankments during an earthquake. Geotext Geomembr 29(3):222–232
Xu C, Xu XW (2013) Controlling parameter analyses and hazard mapping for earthquake-triggered landslides: an example from a square region in Beichuan County, Sichuan Province China. Arab J Geosci 6(10):3827–3839
Xu C, Shyu JBH, Xu XW (2014a) Landslides triggered by the 12 January 2010 Port-au-Prince, Haiti, Mw = 7.0 earthquake: visual interpretation, inventory compiling, and spatial distribution statistical analysis. Nat Hazards Earth Sys 14(7):1789–1818
Xu C, Xu XW (2014) Statistical analysis of landslides caused by the Mw 6.9 Yushu, China, earthquake of April 14, 2010. Nat Hazards 72(2):871–893
Xu C, Xu XW, Shyu JBH, Zheng WJ, Min W (2014b) Landslides triggered by the 22 July 2013 Minxian–Zhangxian, China, Mw 5.9 earthquake: inventory compiling and spatial distribution analysis. J Asian Earth Sci 92:125–142
Xu C, Xu XW, Yao X, Dai FC (2014c) Three (nearly) complete inventories of landslides triggered by the May 12, 2008 Wenchuan Mw 7.9 earthquake of China and their spatial distribution statistical analysis. Landslides 11(3):441–461
Yaghmaei-Sabegha S, Tsang HH (2011) An updated study on near-fault ground motions of the 1978 Tabas, Iran, earthquake (Mw = 7.4). Sci. Iran 18(4):895–905
Yu YZ, Deng LJ, Sun X, Lu H (2008) Centrifuge modeling of a dry sandy slope response to earthquake loading. Bull Earthq Eng 6(3):47–461
Yu YZ, Deng LJ, Sun X, Lu H (2010) Centrifuge modeling of dynamic behavior of pile-reinforced slopes during earthquakes. J Cent South Univ Technol 17(5):1070–1078